An Access Modelling-based De-embedding Method for High-frequency Characterization of Uni-traveling carrier Photodiodes

Djeber Guendouz, Marina Deng, Mukherjee Chhandak, Christophe Caillaud, Patrick Mounaix, Magali de Matos, Cristell Maneux

Access Modelling-based De-embedding Method for High-frequency Characterization of Uni-traveling carrier Photodiodes

Djeber Guendouz[#1], Marina Deng[#2], Chhandak Mukherjee[#3], Christophe Caillaud[*4], Patrick Mounaix[#5], Magali De Matos[#6] and Cristell Maneux[#7].

[#] IMS Laboratory, University of Bordeaux, CNRS UMR 5218, 33405 Talence, France;

*III-V Lab, A Joint Lab between Nokia Bell Labs, Thales Research & Technology and CEA-LETI, 91767 Palaiseau, France;

{[1]djeber.guendouz, [2]marina.deng, [3]chhandak.mukherjee, [5]patrick.mounaix, [6]magali.dematos, [7]cristell.maneux}@ims-bordeaux.fr, [4]christophe.caillaud@3-5lab.fr

***Abstract* — This paper presents a new one-port de-embedding method demonstrated on a uni-traveling carrier photodiode (UTC-PD) technology for reliable on-wafer high frequency characterization. This method is based on small-signal modelling of RF pads and access lines connected to the active area of the UTC-PD. The new method has been investigated, validated and compared to conventional methods up to 110 GHz. Moreover, the extraction of electrical equivalent circuit elements of the UTC-PD has been validated and compared with conventional methods up to 110 GHz.**

***Keywords* — Test structures; on-wafer HF; hybrid electronic photonic systems; UTC-PD; de-embedding method; measurements; compact model; S-parameter.**

I. Introduction

Integrated hybrid electronic photonic systems (IHEPSs) are one of the most promising candidates for beyond 5G wireless telecommunications in the coming years [1]. This is due to several advantages, namely, high bandwidth and efficient transmission capacity low losses. For example, wireless telecommunications based on IHEPSs can be composed of a laser source, a modulator and a photodiode connected to an antenna for the transmission part. For the reception part of such a system, a Schottky diode can be used [2]. In IHEPSs, photodetectors play a major role. Among these photodetector technologies, the most promising are the uni-traveling carrier photodiodes (UTC-PD) which only rely on electron transport [3]. This has significantly improved its saturation power and bandwidth compared to PIN photodiodes [3]. As a result, UTC-PDs have become a key element for the emerging electronic-photonic technologies operating in the millimetre-wave frequency band. Reliable characterization and accurate modelling of these devices are therefore essential to enable the design of IHEPSs [4]. At high frequencies, the accuracy of the de-embedding method, that sets the measurement reference plane at the device terminals, is of utmost importance. In case of one-port active devices, such as UTC-PDs, de-embedding techniques are rarely studied and conventional methods are not readily compatible with all types of pads and access designs [5][6]. To overcome the limitations of existing methods, in this work, we propose a new one-port de-embedding method applied to a UTC-PD technology, based on the extraction of the small-signal electrical circuit of the pads and access lines specific to these devices. For method validation, we have compared the de-embedded RF measurements with compact model simulation of the UTC-PDs. Afterwards, we compare the results with existing conventional methods up to 110 GHz depicting that our proposed method offers a more reliable de-embedding over the entire frequency range. The rest of the paper is organised as follows: Section II details our access modelling based de-embedding approach; Section III compares results from different de-embedding method followed by model validation; finally, Section IV draws the conclusions.

II. Access Modelling and De-Embedding Technique

A. Test Structures Description

The UTC-PD under test have been fabricated by III-V Lab. The UTC-PD structure is formed by a mesa connected to a waveguide by evanescent coupling. The mesa is composed of an active region. This active region is created mainly by the juxtaposition of a p-doped absorption layer and an n-doped collection layer (Fig. 1a and Fig. 1b). The small-signal electrical equivalent circuit of the UTC-PD (Fig. 1c) is mainly composed of a junction capacitance, C_j, which models the p-n junction of the active region and a resistance, R_s, which models the doped semiconducting layers and metal contacts. The mesa device can be biased via the P^+ and N^+ doped contacts, above and below it, respectively. On both sides of the mesa, the access lines are formed, which are connected up to the GSG pads.

The layout of the pad and the access regions of this technology is presented in Fig. 1d. The signal pad has a size of 75x80 μm^2 with a pitch of 150 µm between the signal and ground pads. The pads are connected to access regions with 50 Ω CPW transmission lines which then end on a mesa bridge.

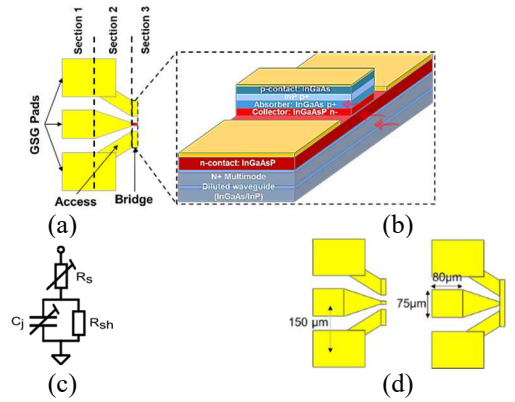

Fig. 1. (a) Schematic of the UTC-PD structure (b) cross section of the UTC-PD active region (c) basic electrical equivalent circuit of the UTC-PD (d) complete Open and Short test structures.

In order to remove the contributions of pads and accesses and in order to obtain the intrinsic characteristics of the UTC-PDs, complete (including the mesa bridge accesses) Open and complete Short test structures have been designed and characterized.

The complete Open and complete Short test structures are ideally modelled by a capacitance and an inductance respectively. Fig. 2 shows that this approximation is valid only up to 40 GHz, beyond which there is a frequency dependence of these electrical equivalent elements. The observed behaviour is more likely equivalent to a distributed electrical network.

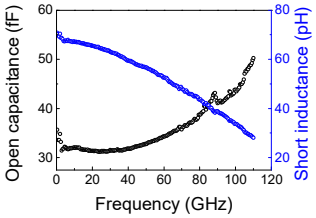

Fig. 2. Extraction of parasitic equivalent capacitance and inductance of the complete Open and Short test structures.

In order to model the later, complementary test structures have been designed and fabricated. These include, a Pad-Short and a Pad-Open (Fig. 3a) structures for the extraction of inductive and capacitive parasitic due to the pads, mesa-free Short and Open (Fig. 3b) structures for the extraction of the inductive, resistive and capacitive parasitics caused by the access lines. The complete Open and Short test structures are used for the extraction of inductive and capacitive parasitic caused by the mesa. The more detailed study will be presented in the next section.

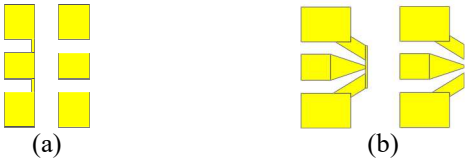

Fig. 3. Complementary test structures: (a) Pad-Short and Pad-Open (b) mesa-free Short and mesa-free Open.

B. De-embedding Procedures

There are mainly two de-embedding methods dedicated to these RF type of test structures. The first method is the conventional Open-Short de-embedding Method [5]. It consists of subtracting the contribution of the capacitance equivalent from the Open and the inductance equivalent from the Short. The intrinsic impedance, Z_{INT}, of the UTC-PD can be determined by the equation (1):

$$Z_{INT} = (Y_M - Y_O)^{-1} - (Y_S - Y_O)^{-1} \quad (1)$$

Where Y_M, Y_S and Y_O are the device, short and open Y-parameters, respectively.

The second method, known as S-parameter based de-embedding method [6], relies on determining the four S-parameter matrix of the pads and access (Fig. 4). For this, an Open and a Short test structure are necessary. For this method the property of the passivity of the accesses is taken into account in order to reduce the matrix elements $(S_{12} = S_{21})$. Also, an assumption of the symmetry of the accesses is considered$(S_{11} = S_{22})$. Such an assumption cannot be verified on a one-port test structures, and therefore may introduce errors in the de-embedding process. This is further investigated in [7]. After determining and simplifying the S-parameter matrix by using the properties of the test structures Open $(|\Gamma_{UTC-PD}| = 1)$ and Short$(|\Gamma_{UTC-PD}| = -1)$, the intrinsic reflection coefficient of the UTC-PD can be simplified as (2):

$$\Gamma_{UTC\text{-}PD} = \frac{\Gamma_O+\Gamma_S-2\Gamma_M-\Gamma_M(\Gamma_O-\Gamma_S)}{2\Gamma_O\Gamma_S+\Gamma_S-\Gamma_O-\Gamma_M(\Gamma_O+\Gamma_S)} \quad (2)$$

Where Γ_O and Γ_S are the reflection coefficients of the Open and Short test structures respectively, and Γ_M is the total measured reflection coefficient of the UTC-PD.

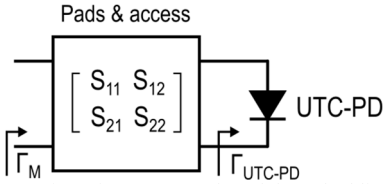

Fig. 4. Representation of S-parameter based de-embedding method.

The new de-embedding method proposed in this work relies on the S-parameter matrix. All four matrix elements have been taken into account and no simplifications have been made, i.e. without the assumption of symmetry of the access that can introduce errors. In order to determine the matrix elements, construction of an electrical equivalent circuit of the pads and of the access lines is necessary. Then a two-port simulation can be performed to determine its four matrix elements.

The global equivalent circuit of the pads and the access has three sections as shown in Fig. 5a. The first section represents the electrical equivalent circuit of the pads. The equivalent parasitic elements of the pads can be determined from the Pad-Short and the Pad-Open test structures and their equivalent circuits (Fig. 5b and Fig. 5c). The inductive element is modelled by an inductance, L_{pad}, which can be determined from the Pad-Short reflection coefficient, $\Gamma_{Pad-Short}$, converted to impedance, $Z_{Pad-Short}$. C_{pad} can be determined from Pad-Open reflection coefficient $\Gamma_{Pad-Open}$ converted to admittance $Y_{Pad-Open}$ and then de-embedded from the pad inductances.

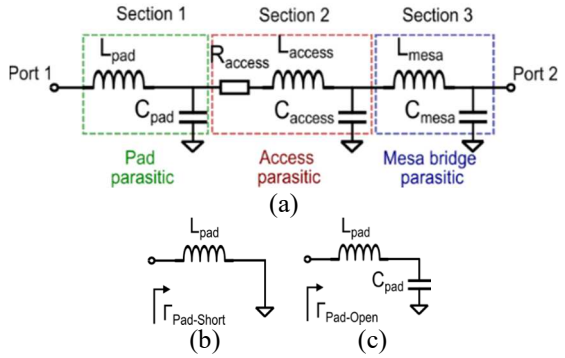

Fig. 5. (a) Global electrical equivalent circuit of the pads and the access of the UTC-PD; (b) electrical equivalent circuit of the Pad-Short (c) electrical equivalent circuit of the Pad-Open.

The second section represents the mesa-free access regions. The corresponding parasitic elements can be determined from the mesa-free Short and mesa-free Open test structures through their respective equivalent circuits (Fig. 6a and Fig. 6b). The parasitic lumped elements, R_{access}, L_{access} and C_{access} can be determined from reflection coefficients, $\Gamma_{mesa-free-Short}$ and $\Gamma_{mesa-free-Open}$, de-embedded from pad parasitic elements.

Fig. 6. Electrical equivalent circuit of the mesa-free access test structures (a) Short (b) Open.

The third section is equivalent to the mesa bridge access lines. The parasitic elements can be determined from the complete Short and complete Open test structures and their equivalent circuits (Fig. 7a and Fig. 7b). The parasitic lumped elements, L_{mesa} and C_{mesa} can be determined from reflection coefficients, Γ_{Short} and Γ_{Open}, de-embedded from the parasitic contributions of the pads and the mesa-free access regions.

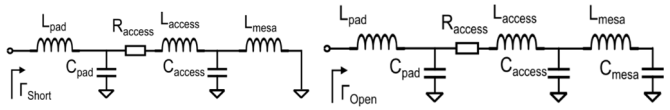

Fig. 7. Electrical equivalent circuits of the complete (a) Short test structure (b) Open test structure.

Once the equivalent circuit of the pads and the access regions is determined, the S-parameter matrix can be determined and the reflection coefficient of the UTC-PD can therefore be expressed by the following expression (3):

$$\Gamma_{UTC-PD} = \frac{S_{11}-\Gamma_M}{S_{11}S_{22}-S_{22}\Gamma_M-S_{12}S_{21}} \quad (3)$$

Where, S_{ij} are the S-parameter matrix elements and Γ_M is the total measured reflection coefficient.

III. Results And Discussions

In order to investigate the validity of the previously discussed de-embedding methods, measurements of the S-parameters were performed on a UTC-PD with an active area of 5x25 µm^2 and on all proposed test structures: Pad-Open and Pad-Short, mesa-free Open and mesa-free Short, complete Open and complete short.

An off-wafer SOLT calibration on CS-S substrate was used to set the measurement reference planes at the probe tips. The on-wafer S-parameter measurements were carried out up to 110 GHz using an Agilent E8361 PNA, with frequency extenders for the 67–110 GHz frequency range, using Picoprobe tips.

A. De-embedding with Conventional methods

The two conventional de-embedding methods have been applied on the S-parameter measurements of the UTC-PDs up to 110 GHz. The results are shown in Fig. 8, which are compared with compact model simulation results of the intrinsic UTC-PD. A good agreement is observed until 40 GHz for both the amplitude and the phase. Beyond that, the de-embedded S-parameters deviate from the model predictions.

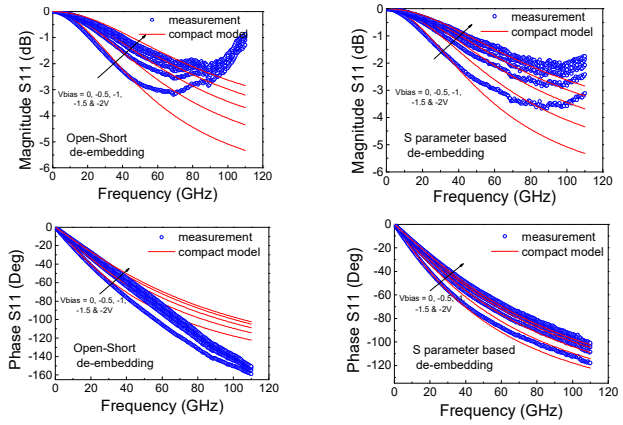

Fig. 8. Magnitude and phase of de-embedded S_{11} comparing measurement (symbol) and compact model simulations (line) for a UTC-PD with an active area of 5x25 µm^2 using (a) Open-Short method (b) S-parameter based method.

B. De-embedding with the proposed method up to 110 GHz

Following the procedure explained in the last section, the new de-embedding method has also been applied on the measurements of the S-parameters. The parasitic elements were determined for each segment of the electrical network. Fig. 9 shows the mesa inductance, L_{mesa}, extracted from Γ_{Short}. The extracted value is overestimated since it includes a return inductance to ground. A correction to this value has been made by optimising the simulated value on the imaginary part of the admittance, Y_{Open}/ω.

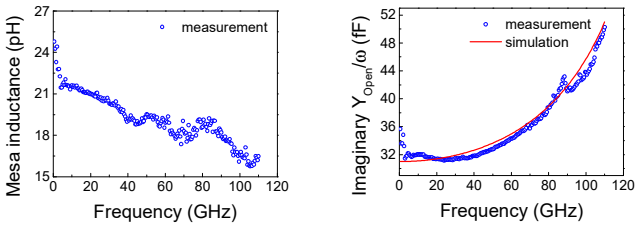

Fig. 9. (a) Frequency dependence of the complete Short inductance and resistance (b) imaginary part of the admittance of the complete Open test structure.

C. *Validation on UTC-PD Characterization Up to 110 GHz*

Following the procedure explained in the section above, the parasitic elements were determined for each segment of the electrical network. The set of the parasitic elements equivalent to the pads and access model are summarized in table I.

Table 1. Extracted equivalent elements values for the pad and the access.

L_{pad}	C_{pad}	R_{access}	L_{access}	C_{access}	L_{mesa}	C_{mesa}
18pH	15fF	1Ω	28pH	11fF	5pH	5fF

The new de-embedding method has been applied on the one port S-parameter measurements performed on the UTC-PD technology under test. The de-embedding results and the compact model simulations are presented in Fig. 10a and Fig. 10b, showing the amplitude and the phase of the S_{11}, respectively. The measurements and the model predictions are in very good agreement over the [0-110 GHz] range for all bias voltages ranging from 0 to -2 V.

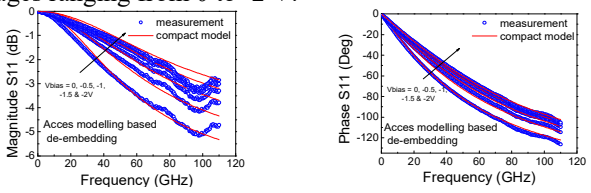

(a) (b)

Fig. 10. De-embedded measurements (symbol) and compact model simulations of (line) S_{11} for a UTC-PD with active area of 5x25 μm²: (a) magnitude (b) phase up to 110 GHz for biases ranging from 0 to -2V.

An extraction of the electrical equivalent circuit elements of the intrinsic UTC-PD model, namely the junction capacitance, C_j, and the series resistance, R_S, (real part of Z_{11} at high frequency) is presented in Fig. 11, comparing the three de-embedding methods discussed in this work.

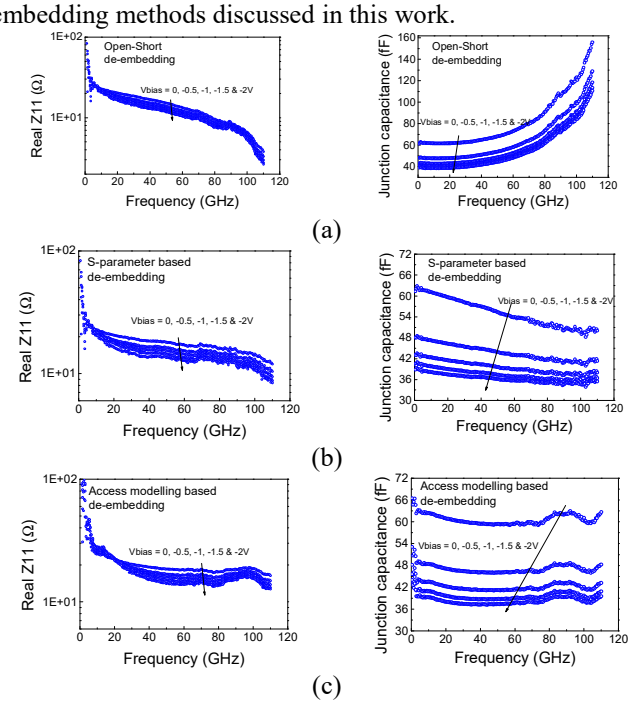

(a)

(b)

(c)

Fig. 11. De-embedded real part of Z_{11} and junction capacitance of the UTC-PD as function of frequency obtained using the (a) Open-Short method (b) S-parameter based method (c) access modelling-based method.

The results obtained with the two conventional de-embedding methods show a frequency dependence of the equivalent circuit elements (Fig. 11a and Fig. 11b). Among the two conventional methods, the S-parameter based method shows relatively better results in this frequency range, given that only one type of test structures, namely the complete Open and complete Short, are available. Provided that we have all the test structures necessary to construct the distributed model, the access modelling-based method remains more accurate and reliable up to 110 GHz (Fig. 11c), compared to conventional methods. It should be noted that a 3-dB cut-off frequency of 44 GHz has been extracted at -2V for this device.

IV. CONCLUSION

In this paper, we have evaluated two conventional de-embedding methods, namely the Open-Short method and the S-parameter based method. The results show that these methods are not compatible for all types of test structures and are no longer valid above 40 GHz, with however slightly better result for S-parameter based method. To provide accurate de-embedding above 40 GHz, we have proposed a new access modelling-based de-embedding method that has been validated against S-parameter measurements of a UTC-PD. The results obtained from this method shows good accuracy in comparison with the compact model simulations up to 110 GHz. Furthermore, we have also extracted the small-signal equivalent circuit parameters of the UTC-PD with the three de-embedding methods. Unlike the two conventional methods that give frequency-dependent values and are not representative of the UTC-PD equivalent circuit model, our method allows to extract frequency-independent model parameters up to 110 GHz. Our proposed method can prove to be quite essential for on-wafer high-frequency characterization of UTC-PDs, especially beyond 110GHz.

ACKNOWLEDGMENT

This work was supported partly by the European project H2020 5G-PHOS (no. 761989), http://www.5g-phos.eu/.

REFERENCES

[1] C. Mukherjee *et al.*, "Towards Monolithic Indium Phosphide (InP)-Based Electronic Photonic Technologies for beyond 5G Communication Systems," *Appl. Sci.*, vol. 11, no. 5, p. 2393, Mar. 2021.

[2] K. Sengupta, T. Nagatsuma, and D. M. Mittleman, "Terahertz integrated electronic and hybrid electronic–photonic systems," *Nat. Electron.*, vol. 1, no. 12, pp. 622–635, Dec. 2018.

[3] T. Ishibashi, N. Shimizu, S. Kodama, H. Ito, T. Nagatsuma, and T. Furuta, "Uni-Traveling-Carrier Photodiodes," *Ultrafast Electron. Optoelectron.*, pp. 166–168, 1997.

[4] C. Mukherjee *et al.*, "Efficient compact modelling of UTC-photodiode towards terahertz communication system design," *Solid. State. Electron.*, vol. 170, no. April, p. 107836, Aug. 2020.

[5] M. C. A. M. Koolen, "On-wafer high-frequency device characterization," *Microelectron. Eng.*, vol. 19, no. 1–4, pp. 679–686, Sep. 1992.

[6] H. Xu and E. Kasper, "A de-embedding procedure for one-port active mm-wave devices," *2010 10th Top. Meet. Silicon Monolith. Integr. Circuits RF Syst. SiRF 2010 - Dig. Pap.*, pp. 37–40, Jan. 2010.

[7] D. Konstantinou, C. Caillaud, S. Rommel, U. Johannsen, and I. Tafur Monroy, "Investigation of de-embedding techniques applied on uni-traveling carrier photodiodes," *Int. J. Microw. Wirel. Technol.*, pp. 1–13, Mar. 2021.